Supplementary Materials for

Structure of the basal edge dislocation in ZnO

Atsutomo Nakamura [1,*], **Eita Tochigi** [2], **Ryota Nagahara** [1], **Yuho Furushima** [1], **Yu Oshima** [1], **Yuichi Ikuhara** [2,3], **Tatsuya Yokoi** [1] **and Katsuyuki Matsunaga** [1,3]

[1]   Department of Materials Physics, Nagoya University, Furo-cho, Chikusa-ku, Nagoya 464-8603, Japan

[2]   Institute of Engineering Innovation, University of Tokyo, 2-11-16 Yayoi, Bunkyo-ku, Tokyo113-8686, Japan

[3]   Nanostructures Research Laboratory, Japan Fine Ceramics Center, 2-4-1, Mutsuno, Atsuta-ku, Nagoya 456-8587, Japan

[*]   Correspondence: anaka@nagoya-u.jp

1. Derivation of the equation (1)

As mentioned in the main text, the attractive force originated from energy of a stacking fault between partials is balanced with the elastic repulsive forces between the partials. Therefore, stacking fault energy can be estimated by calculating the elastic force acting between the partial dislocations. Here note that the $1/3[2\bar{1}\bar{1}0]$ edge dislocation in ZnO dissociates into two partial dislocations of $b_1 = 1/3[10\bar{1}0]$ and $b_2 = 1/3[1\bar{1}00]$. The $1/3[10\bar{1}0]$ partial dislocation has $1/6[2\bar{1}\bar{1}0]$ edge component and $1/6[01\bar{1}0]$ screw component, while the $1/3[1\bar{1}00]$ partial dislocation has $1/6[2\bar{1}\bar{1}0]$ edge component and $1/6[0\bar{1}10]$ screw component. Namely, the two partial dislocations have the same edge component and the opposite screw component. In this case, according to the Peach-Koehler's equation, the relation between the repulsive force F and the stacking fault energy γ is given by the following equation,

$$F = \gamma = \frac{\mu b_e{}^2}{2\pi r\,(1-\nu)} - \frac{\mu b_s{}^2}{2\pi r} \quad \cdots\cdots \quad (S1),$$

where the μ is the shear modulus, ν is the Poisson' ratio, b_e and b_s are the magnitude of the edge and screw components of the partial dislocations and r is the separation distance. This Eq. (S1) is available to two parallel infinite dislocations with equal magnitude of Burgers vectors. A similar equation is described in *p. 112* of *Ref. 10* by more general shape. The first and second members of the Eq. (S1) represent the forces due to edge and screw components, respectively. Also, the negative sign of the second member of the Eq. (S1) attributes to the opposite sign of the screw components. The Burgers vectors of the partial dislocations are inclined at 60º with respect to the dislocation line, and thus b_e and b_s can be represented as follows,

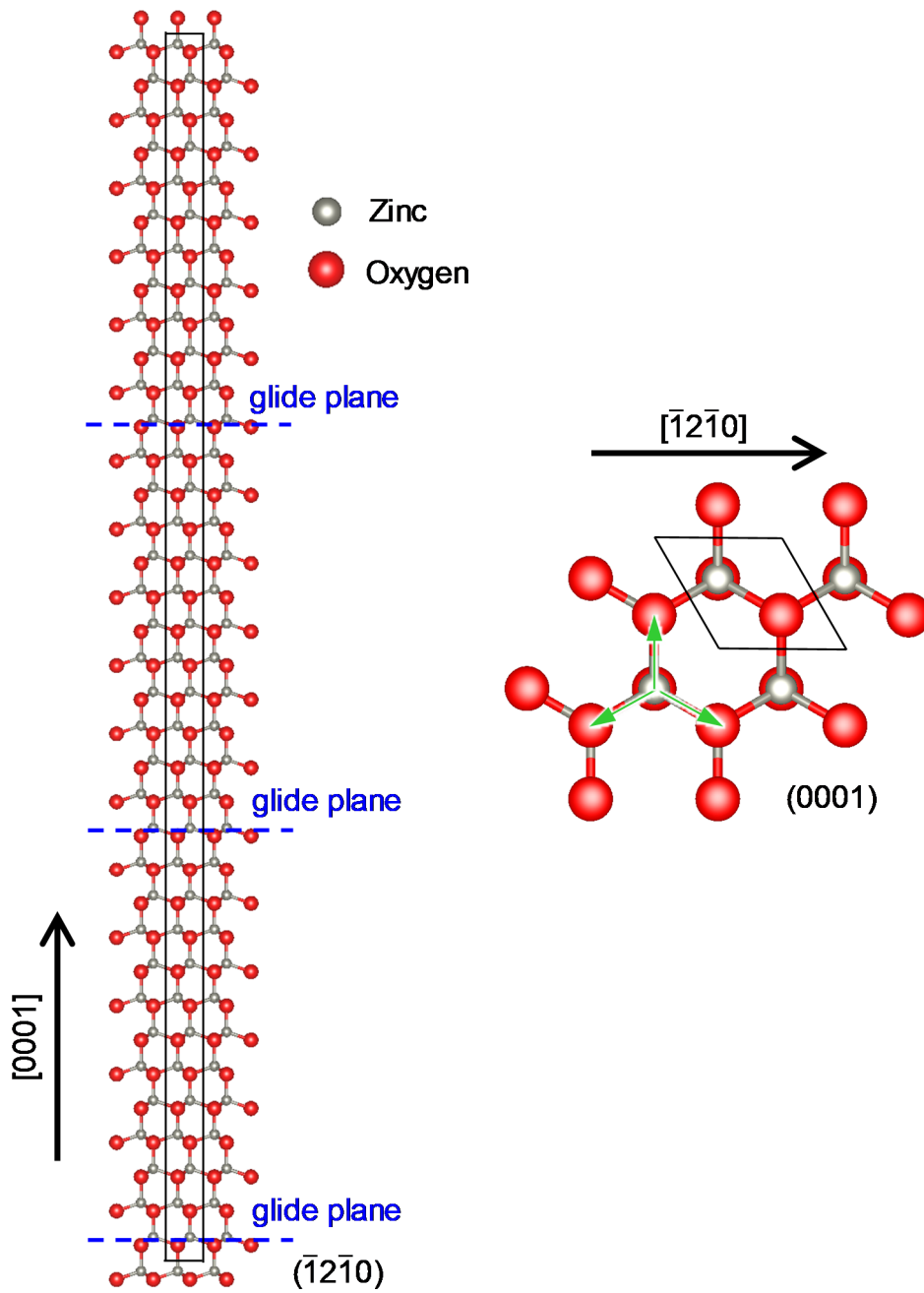$$b_e = \frac{\sqrt{3}}{2}\, b_p \quad \cdots\cdots \quad (S2)$$

and

$$b_s = \frac{1}{2}\, b_p \quad \cdots\cdots \quad (S3),$$

where b_p is the magnitude of Burgers vectors of the partial dislocations. By submitting the equations (S2) and (S3) into the equation (S1), the following equation (1) can be derived.

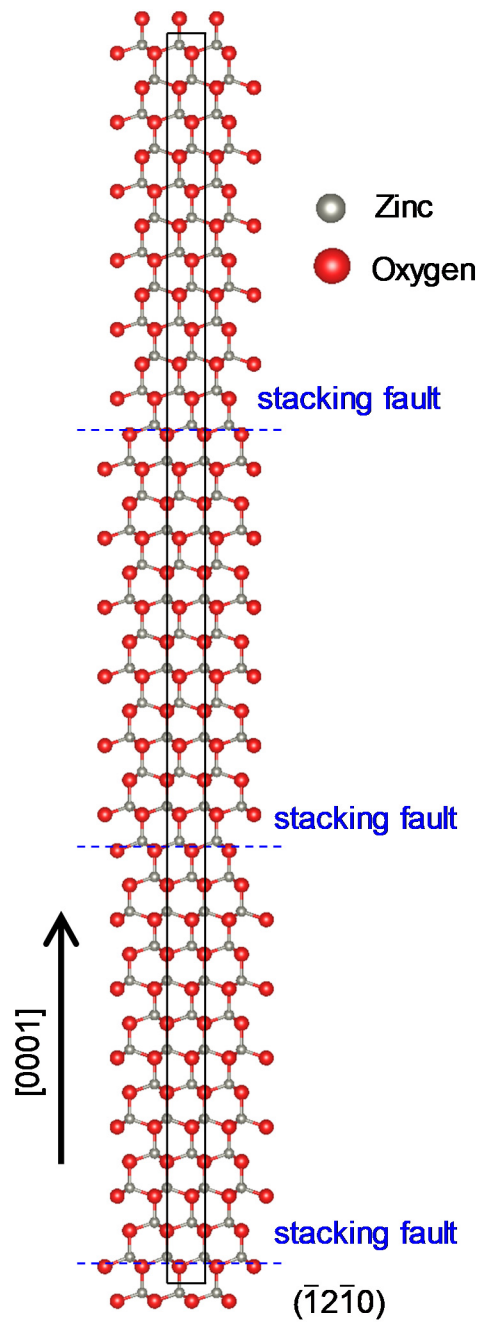$$\gamma = \frac{\mu b_p{}^2(2+\nu)}{8\pi r\,(1-\nu)} \quad \cdots\cdots \quad (1)$$

2. Initial and relaxed structures of supercells for the DFT calculations

Since the main text does not include detailed structures of supercells for the DFT calculations in this study, a part of such structures of supercells will be shown so as to assist understanding of supercell structures employed for the DFT calculations. Figure S1 (a) and (b) show the [$\bar{1}2\bar{1}0$] view of initial structure containing a supercell employed for the (0001) stacking faults and the [0001] view of the structure, respectively. The regions surrounded by black solid lines in the figures correspond to a supercell. In the case of DFT calculations on polar crystals, polar surfaces should not be involved in the supercells, because the polar surfaces of the atomic slabs often induce spurious electric-dipole interactions normal to the slab surfaces. The wurtzite structure of ZnO corresponds to a polar crystal structure. Therefore, we constructed supercells without vacuum layers. Also, the wurtzite structure does not have a mirror symmetry but has a three-fold symmetry around the [0001] axis. Accordingly, the three atomic slabs in a supercell are rigidly shifted by a displacement toward three equivalent directions, resulting in the generation of three equivalent stacking faults without vacuum layers in a supercell. Similar calculations also can be seen in *Refs. 24* and *25*. Figure S2 shows the [$\bar{1}2\bar{1}0$] view of relaxed structure of the (0001) stacking fault with the fault vector of 1/3<10$\bar{1}$0> as a reference. It can be seen that the three stacking faults have the equivalent structure. Figure S3 shows the [0001] view of initial structure containing a supercell employed for calculations of the (2$\bar{1}\bar{1}$0) stacking faults. Since the {2$\bar{1}\bar{1}$0} surfaces in the wurtzite structure are not polar, a vacuum layer is inserted in a supercell so as to reduce the number of atoms demanded for the calculations. The region surrounded by black solid lines in the figure indicates the size of the employed supercell. Figure S4 shows the [0001] view of relaxed structure of the (2$\bar{1}\bar{1}$0) stacking fault with the fault vector of 1/2[01$\bar{1}$1] as a reference. Also, Fig. S5 shows energies of the (2$\bar{1}\bar{1}$0) stacking faults with the fault vectors of 1/2[01$\bar{1}$1] and 1/2[01$\bar{1}$0], which were checked by longer supercells with more atoms. As a result, energy convergence was well satisfied with regard to the employed supercells as shown in Fig. S5. We should note that all the initial structures of the employed supercells were prepared using our original script from the optimized bulk perfect structure.
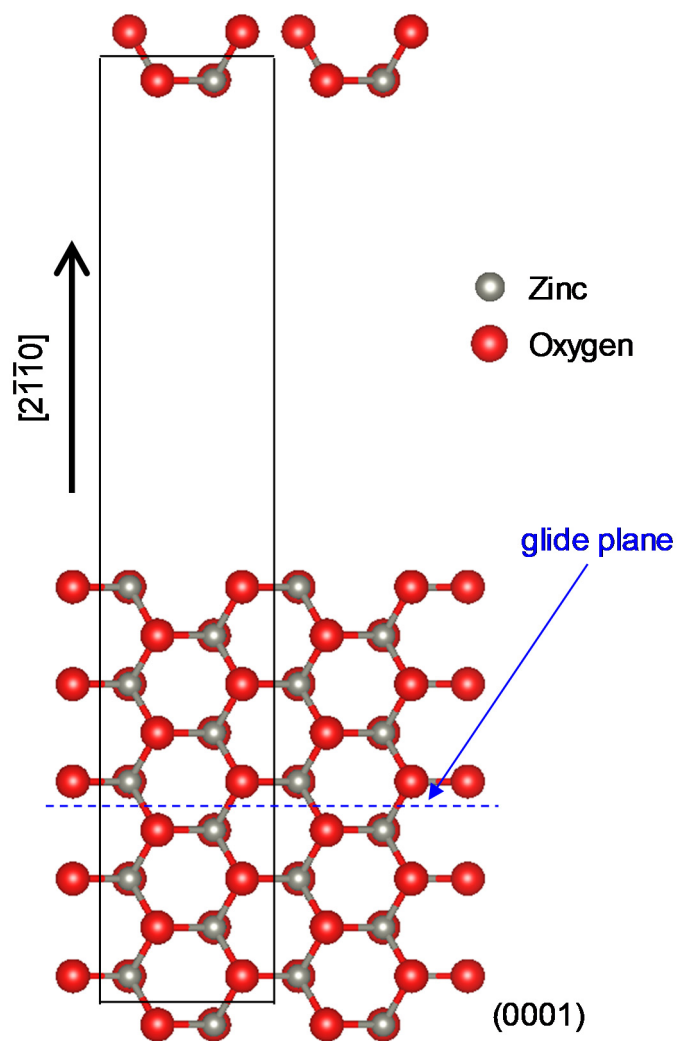
Figure S1

(a) The [$\bar{1}2\bar{1}0$] view of initial structure containing a supercell without displacements for the (0001) stacking faults. (b) The [0001] view of the initial structure. The three green arrows in the figure shows three equivalent <10$\bar{1}$0> directions as a reference. The regions surrounded by black solid lines in the figures correspond to a supercell.
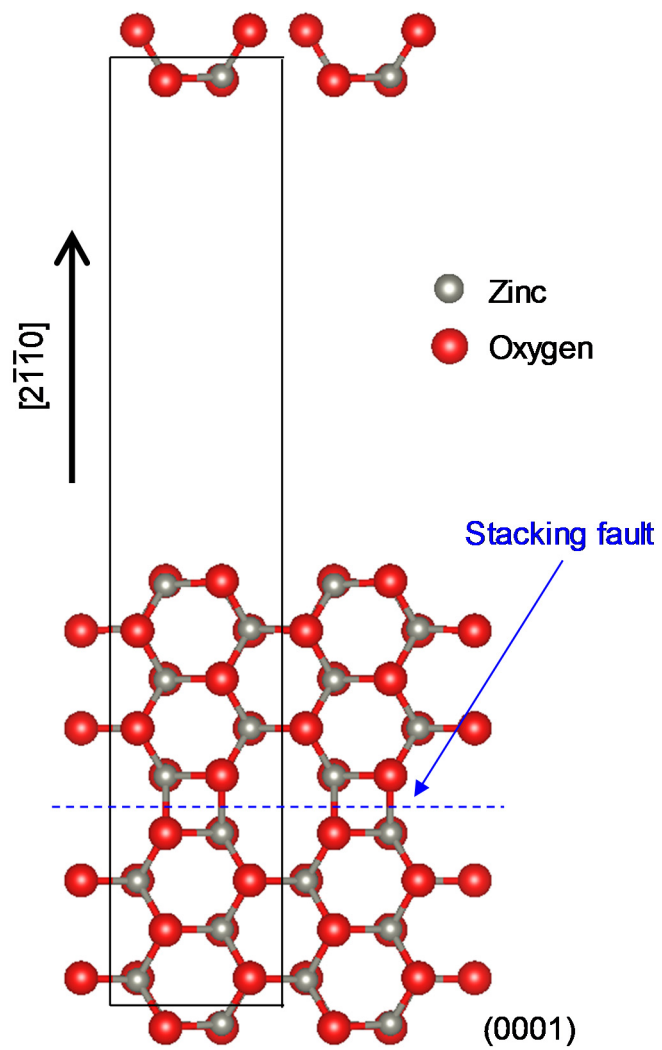
Figure S2
The [$\bar{1}2\bar{1}0$] view of initial structure containing three equivalent stacking faults with the fault vectors of 1/3<10$\bar{1}$0> before optimization.
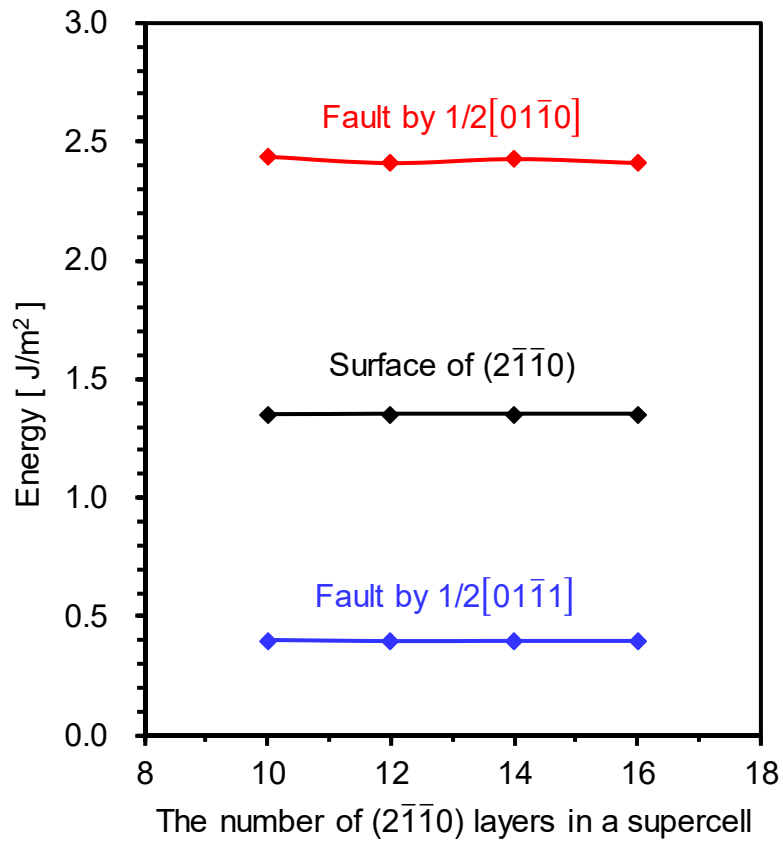
Figure S3
The [0001] view of initial structure containing a supercell employed for calculations of the $(2\bar{1}\bar{1}0)$ stacking faults. The region surrounded by black solid lines in the figure indicates the size of the employed supercell.

Figure S4
The [0001] view of relaxed structure of the (2$\bar{1}\bar{1}$0) stacking fault with the fault vector of 1/2[01$\bar{1}$1] after optimization.

Figure S5

Convergence of energies of the (2$\bar{1}\bar{1}$0) stacking faults with the fault vectors of 1/2[01$\bar{1}$1] and 1/2[01$\bar{1}$0] as a function of the number of (2$\bar{1}\bar{1}$0) layers.